



Published in final edited form as:

J Mol Biol. 2011 January 14; 405(2): 531–547. doi:10.1016/j.jmb.2010.11.009.

Structural insight into the expanded PCB-degrading abilities of a biphenyl dioxygenase obtained by directed evolution

Pravindra Kumar^{1,4,†}, Mahmood Mohammadi^{2,†}, Jean-François Viger^{2,†}, Diane Barriault², Leticia Gomez-Gil³, Lindsay D. Eltis³, Jeffrey T. Bolin¹, and Michel Sylvestre^{2,*}

¹Department of Biological Sciences and Center for Cancer Research, Purdue University, West Lafayette, IN., 47907, USA

²Institut National de la Recherche Scientifique (INRS-Institut Armand-Frappier), Laval, QC, H7V 1B7, Canada

³Departments of Microbiology and Biochemistry, Life Sciences Institute, University of British Columbia, Vancouver, BC, V6T 1Z3, Canada

⁴Department of Biotechnology, Indian Institute of Technology, Roorkee-247667, India

Abstract

The biphenyl dioxygenase of *Burkholderia xenovorans* LB400 is a multicomponent Rieske-type oxygenase (RO) that catalyzes the dihydroxylation of biphenyl and many polychlorinated biphenyls (PCBs). The structural bases for the substrate specificity of the enzyme's oxygenase component (BphAE_{LB400}) are largely unknown. BphAE_{p4}, a variant previously obtained through directed evolution, transforms several chlorobiphenyls, including 2,6-dichlorobiphenyl, more efficiently than BphAE_{LB400} yet differs from the parent oxygenase at only two positions: T335A/F336M. Herein, we compare the structure of BphAE_{LB400} and BphAE_{p4} and examine the biochemical properties of two BphAE_{LB400} variants with single substitutions, T335A or F336M. Our data show that residue 336 contacts the biphenyl and influences the regiospecificity of the reaction, but does not enhance the enzyme's reactivity toward 2,6-dichlorobiphenyl. By contrast, residue 335 did not contact biphenyl, but contributed significantly to expansion of the enzyme's substrate range. Crystal structures indicate that Thr335 imposes constraints through hydrogen bonds and non-bonded contacts to the segment from Val320 to Gln322. These contacts are lost when Thr is replaced by Ala, relieving intramolecular constraints and allowing for significant movement of this segment during binding of 2,6-dichlorobiphenyl, increasing the space available to accommodate the doubly-*ortho*-chlorinated congener 2,6-dichlorobiphenyl. This study provides important insight about how ROs can expand substrate range through mutations that increase the plasticity and/or mobility of protein segments lining the catalytic cavity.

© 2011 Elsevier Ltd. All rights reserved.

*Corresponding author address: Michel Sylvestre, Institut National de la Recherche Scientifique (INRS-Institut Armand-Frappier), Laval, Québec, H7V 1B7, Canada. Phone: 450-687-5010; FAX: 450-686-5501; Michel.Sylvestre@iaf.inrs.ca.

†P.K., M.M. and J.F.V. contributed equally to the manuscript.

Present address: M.M., Département de génie informatique et génie logiciel, École Polytechnique de Montréal, C.P. 6079, succ. Centre-ville, Montréal, QC, H3C 3A7, Canada ; J.F.V., Biofloral, 675 Montée St-François, Laval, QC, H7C 2S8, Canada

Publisher's Disclaimer: This is a PDF file of an unedited manuscript that has been accepted for publication. As a service to our customers we are providing this early version of the manuscript. The manuscript will undergo copyediting, typesetting, and review of the resulting proof before it is published in its final citable form. Please note that during the production process errors may be discovered which could affect the content, and all legal disclaimers that apply to the journal pertain.

Keywords

Polychlorinated biphenyl; *Burkholderia xenovorans* LB400; enzyme engineering; Rieske-type oxygenase; PCB

Introduction

Biphenyl dioxygenase (BPDO) is a multicomponent Rieske-type oxygenase (RO). As other aryl-hydroxylating dioxygenases it has been extensively studied because it catalyzes the transformation of a range of non-physiological substrates. These include polychlorinated biphenyls (PCBs), which are of environmental concern^{1; 2}, and heterocyclic compounds of pharmaceutical and agrochemical interest^{3; 4; 5; 6}. BPDO catalyzes the first reaction of the bacterial biphenyl catabolic pathway. This three-component system catalyzes the insertion of two oxygen atoms onto vicinal carbons of biphenyl, yielding *cis*-(2*R*,3*S*)-dihydroxy-1-phenylcyclohexa-4,6-diene. In *Burkholderia xenovorans* LB400⁷, the three components are: the oxygenase, BphAE_{LB400}, an heterohexamer comprised of 3 α (BphA_{LB400}) and 3 β (BphE_{LB400}) subunits; the ferredoxin, BphF_{LB400}; and the ferredoxin reductase component, BphG_{LB400} (Fig. 1). Each α subunit of the $\alpha_3\beta_3$ hexamer contains a Rieske-type Fe₂S₂ cluster and a mononuclear iron center⁸. Electrons flow successively from NADH to the FAD center in BphG, thence to the Rieske clusters of BphF and of BphAE, and finally to the mononuclear iron catalytic center. The mechanism of dihydroxylation is thought to be very similar to that of naphthalene dioxygenase (NDO) from *Pseudomonas sp.* NCIB 9816-4⁹.

BPDO_{LB400} is one of the most potent biocatalysts of natural origin for the dioxygenation of chlorobiphenyls¹⁰. However, several di- and trichlorinated biphenyls are poorly transformed by this enzyme, including 2,6-dichlorobiphenyl, one of the major metabolites resulting from the reductive dehalogenation process conducted during anaerobic dehalorespiration^{11; 12}. Moreover, as pointed out by previous authors^{11; 13}, the congeners containing two chlorines in the *ortho* position of a single ring (2,6-dichlorobiphenyls) are strikingly resistant to co-metabolic degradation by aerobic bacteria. Only rare bacteria of natural origin and recombinant bacteria producing engineered BPDOs were shown to transform this congener^{14; 15; 16}.

Recently, the BphAE_{p4} variant was created from BphAE_{LB400} by substitution at two residues, T335A and F336M¹⁵. This variant catalyzes the oxygenation of many PCB congeners, including 2,6-dichlorobiphenyl, more efficiently than BphAE_{LB400}¹⁵. Structures of *Pandorea pnomenus* B-356 BphAE (BphAE_{B356}), of *Rhodococcus jostii* BphA1A2 (BphA1A2_{RHA1}), of *Sphingobium yanoikuyae* B1 (BphA1A2_{B1}) and of cumene and toluene dioxygenases have been reported^{16; 17; 18; 19; 20}. Structural analyses have shown that residue Ile326 of BphA1_{RHA1} (corresponding to Phe336 of BphA_{LB400}) makes contact with the substrate but residue Gly325 of BphA1_{RHA1} (corresponding to Thr335 of BphAE_{LB400}) is too distant to interact directly with substrate. Similarly, residue 377 of BphA_{LB400}^{14; 15; 21; 22} and several others²³ that, according to models of BphAE, have no contact with the substrate, were shown to modulate the reaction turnover rates and regiospecificity toward chlorobiphenyls. However, the mechanisms by which these residues influence the enzyme's catalytic properties remain unclear.

In the classic model of enzyme-substrate interaction as a lock-and-key, the catalytic cavity defines the space that fits exactly the dimension and shape of the substrate, placing its reactive atoms into a productive position toward the catalytic center. This model predicts the enzyme's catalytic cavity can be remodeled to fit a new substrate by altering residues that line the catalytic pocket. However, this model is inadequate for enzymes that bind many

different substrates in a productive orientation, especially those with bulky substituents, such as chlorobiphenyls. Moreover, the mechanisms by which relaxed enzymes such as BPDO evolve to expand their substrate range are still undetermined. Understanding how the residues influencing ROs' specificity and catalytic properties interact with substrate-analogs will help decipher some of the mechanisms by which these relaxed enzymes evolve and will also help design strategies to engineer improved biocatalysts exhibiting expanded substrate specificities. In this study, in an attempt to identify the mutation(s) in BphAE_{p4} that contribute most to its expanded substrate range and to gain more insight into the role played by residues 335 and 336 of BphA_{LB400}, we have examined the biochemical properties of two BphAE_{LB400} variants with single substitutions, T335A or F336M, and we have determined and compared the three dimensional structures of BphAE_{LB400} and its biphenyl-bound form with those of variant BphAE_{p4} and its 2,6-dichlorobiphenyl-bound form.

Results

Metabolism of 2,6-dichlorobiphenyl by BphAE_{LB400} variants

In a previous report BphAE_{p4} (A335M336) was shown to perform better than BphAE_{LB400} (T335F336) toward 2,6-dichlorobiphenyl¹⁵. In this study, we created BphAE_{p401} (A335F336) and BphAE_{p402} (T335M336) to identify which of the two substitutions has greater influence on activity toward 2,6-dichlorobiphenyl. The ability of all enzymes to catalyze the oxygenation of this substrate was assessed using a whole cell assay with IPTG-induced recombinant *Escherichia coli* strains. SDS-PAGE analysis indicated that *E. coli* DH11S pDB31[LB400-*bphFG*] harboring pQE31[*bphAE*_{LB400}] or either one of the recombinant plasmids pQE31[*bphAE*_{p4}], pQE31[*bphAE*_{p401}] or pQE31[*bphAE*_{p402}] produced similar amounts of enzyme (not shown). Furthermore, based on the amount of 2,3-dihydro-2,3-dihydroxybiphenyl monitored after addition of biphenyl to resting cell suspensions of recombinant *E. coli* expressing these enzymes, the mutations did not affect the ability to oxidize biphenyl and no 3,4-dihydro-3,4-dihydroxybiphenyl was produced.

In a previous study it was shown that BphAE_{p4} metabolizes 2,2'-dichlorobiphenyl to generate principally 3,4-dihydro-3,4-dihydroxy-2,2'-dichlorobiphenyl instead of 2,3-dihydroxy-2'-chlorobiphenyl, as produced by BphAE_{LB400}¹⁵. GC-MS analyses of the metabolites generated by cells producing BphAE_{p401} revealed that this mutant yielded 2,3-dihydroxy-2'-chlorobiphenyl as the major metabolite, whereas BphAE_{p402} produced principally the 3,4-dihydro-3,4-dihydroxy-2,2'-dichlorobiphenyl (Fig. 2a). Therefore, the F336M substitution influenced the regioselectivity toward 2,2'-dichlorobiphenyl, but neither of the mutations (F336M or T335A) curtailed the capacity of the enzyme to dihydroxylate this substrate.

In resting a cell assay, after 18 hours of incubation, recombinant *E. coli* cells expressing BphAE_{p4} transformed 25±5% of the initial amount (50 μM) of 2,6-dichlorobiphenyl added to the bacterial suspension, under the same conditions cells expressing BphAE_{p401} transformed 15±3% of this substrate. Cells expressing BphAE_{p402} and those expressing BphAE_{LB400} metabolized 2,6-dichlorobiphenyl very poorly, transforming less than 1% of the substrate to produce trace amounts of metabolites whereas those expressing BphAE_{p4} and BphAE_{p401} clearly produced two metabolites (Fig. 2b). In previous work, BphAE_{B-356}¹⁶ was shown to produce two metabolites from 2,6-dichlorobiphenyl, and the major one was predicted to be 2',3'-dihydro-2',3'-dihydroxy-2,6-dichlorobiphenyl on the basis of the crystal structure of the BphAE_{B-356}:2,6-dichlorobiphenyl complex which was consistent with an *ortho-meta* oxygenation of this substrate. When BphAE_{p4} catalyzed the oxygenation of 2,6-dichlorobiphenyl, GC-MS analysis showed the minor metabolite was the same as the major metabolite produced by BphAE_{B-356}, i.e., 2',3'-dihydro-2',3'-dihydroxy-2,6-dichlorobiphenyl. Analysis of the crystal structure of the BphAE_{p4}:2,6-

dichlorobiphenyl-complex (see below) is consistent with the fact that BphAE_{p4} produces 3', 4'-dihydroxy-3',4'-dihydro-2,6-dichlorobiphenyl as major metabolite. Cells expressing BphAE_{p401} produced the same metabolites as those expressing BphAE_{p4}, but in lower yield: the sum of areas under GC-MS peaks of metabolites was about one third of the value obtained for cells expressing BphAE_{p4}. Moreover, the ratio of the metabolites, and thus the regiospecificity of these enzymes toward 2,6-dichlorobiphenyl, differed significantly.

In summary, of the mutations T335A and F336M, the data indicate T335A contributed more to the increased-reactivity of BphAE_{p4} toward 2,6-dichlorobiphenyl. It is not clear if the F336M mutation alone influences the regiospecificity because the amounts of metabolites produced by cells expressing BphAE_{p402} are too small. However, it is clear that the additional substitution of F336M along with T335A is effective to alter the regiospecificity. Together, these observations suggest that the side chain at position 336 appears to influence the regiospecificity of the enzyme toward 2,6-dichlorobiphenyl.

Crystal structure BphAE_{LB400}: general features

BphAE_{LB400} crystals have the triclinic space group P_1 with unit-cell parameters $a = 132.6$, $b = 132.4$, $c = 133.0$ Å, and $\alpha = 102.6$, $\beta = 102.7$ and $\gamma = 104.6^\circ$. Analysis of the probable protein and solvent content of the unit cell suggested the possibility of twelve $\alpha\beta$ dimers (four $\alpha_3\beta_3$ -hexamers) in the asymmetric unit with a Matthews coefficient $V_M = 2.41$ Å³ Da⁻¹ and a solvent content of 50%; these basic aspects of the crystal packing were confirmed by determination of the structure. Crystallographic data and statistics are reported in Table 1.

The crystal structure of BphAE_{LB400} was refined to final R and R_{free} values of 20.0% and 26.8% at a resolution of 2.5 Å. The final model includes residues Asn18 to Phe143 and Phe153 to Pro459 of the α subunit and Phe9 to Phe188 of the β subunit. The center part of the α subunit (residues 144–152) was excluded from the final model because it was a disordered region and there was no electron density. Triplets of $\alpha\beta$ dimers associate to generate four $\alpha_3\beta_3$ hexamers with non-crystallographic three-fold symmetry. The $\alpha\beta$ dimers as represented by chains AB-CD-EF, GH-IJ-KL, MN-OP-QR and ST-UV-WX respectively form the four functional hexamers. As other aryl-hydroxylating dioxygenases^{16; 17; 18; 24; 25; 26}, BphAE_{LB400} assembles as a mushroom shaped $\alpha_3\beta_3$ hexamer with the α subunits forming the cap and the β subunits forming the stem. As expected, the folds of the α and β subunits are also very similar to those presented by the structures of the homologs referenced above. Each α subunit carries a Rieske-type [2Fe-2S] His₂Cys₂ cluster and coordinates a mononuclear Fe(II) ion via the side chains of conserved His, His, and Asp residues; the Fe also binds one water molecule.

Crystals of BphAE_{LB400} were exposed to solid biphenyl and subjected to crystallographic analysis, which produced a structure of the complex refined to 2.4 Å resolution and a final R -factor of 21.8% ($R_{\text{free}}=25.2\%$) (Table 1). The biphenyl molecule could be identified clearly in initial difference Fourier maps. Binding of biphenyl in the active site and near the mononuclear Fe(II) requires only local structural adjustments and thus did not alter the basic aspects of crystal packing.

Comparison of the crystal structures of native and biphenyl-bound BphAE_{LB400}

The presence of twelve independent $\alpha\beta$ dimers requires analysis of the variations in protein conformation observed in the crystals. Superposition of the twelve native BphAE_{LB400} dimers shows that they are all very similar in the core of the α subunit. This is also the case for the biphenyl-bound enzyme (Fig. 1a of supplementary material). Thus, for either substrate-free or biphenyl-bound BphAE_{LB400}, the C ^{α} atoms of the twelve protomers can be

superposed in pairs with root-mean-square deviation of 0.2–0.4 Å (Supplementary material, Table 1). The average *B*-factor values were 29.2 Å² and 45.9 Å² for the substrate-free and biphenyl-bound forms. The least ordered residues are located at the edges of the molecule (Fig. 2a–h of supplementary material). Among the segments showing greatest disorder, four are of interest.

The segment comprising residues 247–263 of the α subunit is a loop covering the active site mouth, and it corresponds to residues 223–240 of the α subunit of NDO and of BphA1A2_{B1}. In crystal structures of NDO and of BphA1A2_{B1} this segment was significantly displaced upon substrate binding^{24; 26}. However, superposition of the twelve biphenyl-bound BphAE_{LB400} $\alpha\beta$ dimers with the twelve dimers of the substrate-free enzyme does not reveal a consistent change in conformation associated with substrate binding. That is, substrate binding did not impose any specific conformational change on this segment.

The segment comprising residues 280–287 of the α subunit has high *B*-factors in all chains of native and biphenyl-bound forms of BphAE_{LB400} and shows conformational variability. The *B*-factors of all the chains in native BphAE_{LB400} is lower (~ 37 Å²) in comparison to the biphenyl complex of BphAE_{LB400} (~ 50 Å²). These residues correspond to segment 270–277 of BphA1A2_{RHA1}, which was reported to show significant displacement after substrate binding¹⁸; thus this segment might also play a role in substrate binding. However, in contrast to BphA1A2_{RHA1}, we have no evidence this segment is displaced when BphAE_{LB400} binds biphenyl since the dominant conformation is the same in the presence and absence of substrates.

Finally, the N-terminal segment comprising residues 9–17 of the β subunit also exhibits high *B*-factors. In different contexts, this segment interacts with the active site mouth segment 247–263 of an α subunit belonging to a neighboring $\alpha_3\beta_3$ hexamer or it is pulled toward a loop comprised of residues 158–164 of an adjacent β subunit from the same $\alpha_3\beta_3$ hexamer. Thus, for the centrally positioned hexamer MNOPQR, segment 9–17 of chains N, P and R interacts with segment 247–263 of chains A, K and S of dimers AB, KL and ST, respectively. This movement will be discussed further below.

Consistent with an *ortho-meta* dioxygenation of biphenyl, C-2 and C-3 are the biphenyl atoms closest to the Fe atom and in all active sites they are equidistant to it. A water molecule is directly in line between the Fe atom and C-2 atom of biphenyl (Fig. 3). The separation of the Fe atom from C-2/C-3 is in the range of 3.9–4.1 Å for seven of the twelve dimers (AB, CD, EF, MN, QR, UV, WX). For dimers KL and ST the distance is shorter (3.3–3.5 Å) and for dimers GH, IJ and OP it is longer (4.3–4.5 Å). In this work, BphAE_{LB400} was purified under anaerobic conditions and maintained under these conditions for substrate binding. Therefore, the oxidation state of the catalytic iron should not be the cause of these variations, which suggests some adaptability in the region surrounding the catalytic iron.

The position and orientation of the reactive ring of biphenyl appear to be tightly constrained by the surrounding protein atoms. Side chains of residues Gln226, Phe227, Asp230, Met231, His233, Ala234, His323 and Leu333 of the α subunit are located within 4.5 Å of atoms of the reactive ring (see supplementary material Fig. 3a).

In the distal ring pocket of BphAE_{LB400}, five atoms of the non-reactive ring of biphenyl are located within 4.5 Å of multiple protein atoms from Phe384, Phe378, Phe336, His239, Met231, Gly321 and Val287 (see supplementary material Fig 3b). In spite of these multiple contacts, superposition of the twelve $\alpha\beta$ dimers clearly illustrates that the non-reactive ring may access different orientations. These variations do not seem to be associated with equivalent variation in the orientation of the reactive ring, especially the *ortho-meta* C-2/C-3

atoms. Furthermore, the conformations of the residues lining the catalytic pocket remain very similar in all twelve dimers. Altogether, structural analysis shows the catalytic pocket of BphAE_{LB400}, as represented by the crystal structure of the substrate-free enzyme, provides enough space to bind biphenyl in a productive manner without major changes in protein conformation within the catalytic pocket.

Comparison of the crystal structure of BphAE_{LB400} with other BPDs

The superposition of biphenyl-complexed BphAE_{LB400} (dimers AB, CD, EF) with biphenyl-complexed BphA1A2_{RHA1} shows that the relative positions of the residues that coordinate the catalytic iron, His233, His239 and Asn388 in BphAE_{LB400} and His224, His230 and Asn378 in BphA1_{RHA1}, are similar (Supplementary material, Fig. 4). It also shows that carbons C-2 and C-3 of biphenyl align very well although their distance to the catalytic iron is shorter in BphAE_{LB400} than in BphA1A2_{RHA1} and BphA1A2_{B1}^{18; 24}. In the case of BphA1A2_{RHA1}, several residues of the catalytic pocket, such as Leu274 and Ala311, were shown to move significantly after biphenyl binding. Using CASTp²⁷ software, and a probe radius of 1.4Å, we measured an average volume of 1071 Å³ for all twelve αβ dimers of native BphAE_{LB400} and 312 Å³ for BphA1A2_{RHA1}. This suggests the greater side chain displacements observed when BphA1A2_{RHA1} binds to biphenyl might be caused in part by the smaller cavity volume compared to BphAE_{LB400}. Biphenyl-bound BphAE_{LB400} does not superpose as well with BphA1A2_{B1}²⁴ which is structurally more similar to naphthalene than to biphenyl dioxygenases.

Crystal structure of BphAE_{p4}: general features

BphAE_{p4} native crystals were grown in the triclinic space group P_1 with unit cell parameters $a = 132.6$, $b = 132.4$, $c = 133.0$ Å, and $\alpha = 102.6$, $\beta = 102.7$ and $\gamma = 104.6^\circ$, and they diffracted to 2.2 Å. Crystals of the 2,6-chlorobiphenyl-complex were grown in the monoclinic space group $P2_1$ with $a = 86.7$, $b = 276.8$, $c = 93.3$ Å and $\beta = 117.4^\circ$ and diffracted to comparable resolution (Table 1). The BphAE_{LB400} crystal structure was used as a search model to find initial phases for BphAE_{p4} and provided the initial model, which was subsequently refined to final R and R_{free} values of 21.4 and 26.6% at a resolution of 2.2 Å. The final refined model contains residues Asn18 to Phe143 plus Phe153 to Pro459 of the α subunit, residues Phe9 to Phe188 of the β subunit, 145 water molecules, and one glycerol molecule. Quantities and statistics characterizing the diffraction data and the refined model are provided in Table 1.

The structure of native BphAE_{p4} is very similar to that of native BphAE_{LB400}, where triplets of αβ dimers associate to generate four α₃β₃ hexamers possessing non-crystallographic three-fold symmetry. Superposition of all C^α atoms for chains AB and chains CD-WX yielded rmsd values of 0.2–0.4 Å² and the average B -factor was 32.6 Å² (supplementary material, Table 1). The most disordered residues and protein segments were the same as observed for BphAE_{LB400}, including the segments comprising residues Ile247-Lys263 and Glu280-Val287 of the α subunit and 9–17 and 158–164 of the β subunit, as discussed above. In addition, other residues or segments of the α subunit showed variations in position among the twelve dimers. These were His233-His239, Val320-Glu322, Asp388, Lys403-Ala411, Pro423-Tyr433. (supplementary material Fig. 2i–k). As observed for BphAE_{LB400} the flexible N-terminal region (residues 9–17) of the β subunit are having two conformations. In one type of conformation, this segment interacts with the active site mouth of an α subunit belonging to a neighboring α₃β₃ hexamer. This movement is also observed for the native form of BphAE_{p4}. However, in the case of the 2,6-dichlorobiphenyl-bound form of BphAE_{p4}, no dimer interacts with the active site mouth residue and all of them exhibit the second conformation (supplementary material Fig. 3b). On the basis of this observation, it can be postulated that conformational variations of the N-terminal portion of the β subunit

might influence substrate specificity. However, more data is required to support these hypotheses and we will not discuss this further in this work. Nevertheless, the role of the β subunit is not yet clearly understood but, in some experiments, the β subunit was found to influence substrate specificity^{28; 29}.

The crystal structure of the BphAE_{p4}:2,6-dichlorobiphenyl complex contains triplets of $\alpha\beta$ dimers that associate to generate two (ABCDEF and GHIJKL) hexamers in the asymmetric unit. 2,6-Dichlorobiphenyl could be identified clearly in difference Fourier maps in the active sites of the ABCDEF hexamer. However, the active sites of the GHIJKL hexamer did not have sufficient density to justify modeling the substrate. The electron density maps of the catalytic center residues of the native BphAE_{p4} and of its 2,6-dichlorobiphenyl-complex are shown in Fig. 4.

Comparison of the crystal structures of native and substrate-bound BphAE_{p4} and BphAE_{LB400}

When the six $\alpha\beta$ dimers of the BphAE_{p4}:2,6-dichlorobiphenyl complex are superposed, the deviations are small in the core region of the molecule (supplementary material Fig. 1b). The most variable segments are the same as for the native BphAE_{p4}. Superposition of all C α atoms for chain AB and chains CD-WX yielded rmsd values of 0.25–0.36 Å and the average B-factor value was 49.2 Å² (supplementary material Fig. 2l–m).

When chains AB, CD, and EF of the BphAE_{p4}:2,6-dichlorobiphenyl complex were superposed with each other and also with the 12 $\alpha\beta$ dimers of the biphenyl complex of BphAE_{LB400}, it was observed that the orientation of the chlorinated substrate differs from the orientation of biphenyl in BphAE_{LB400}. The non-reactive ring of 2,6-dichlorobiphenyl is shifted toward Gly321 and Met336 (Fig. 5). This shift is correlated with a change in the placement of the reactive ring of 2,6-dichlorobiphenyl, such that the relationship of carbons C-2/C-3 to the Fe is altered. In addition, it appears that the Fe atom and Asp388 withdraw from the substrate (see Fig. 6a) when 2,6-dichlorobiphenyl binds BphAE_{p4}. Such a displacement is not observed when BphAE_{LB400} binds biphenyl (Fig. 6b). An interesting consequence of these movements is that carbons C-2 and C-4 of 2,6-dichlorobiphenyl are positioned at a similar distance from the Fe atom: the distances that separate the *ortho*, *meta* and *para* carbons of 2,6-dichlorobiphenyl from the iron of BphAE_{p4} are on average 4.8 Å, 4.5 Å and 4.9 Å respectively (Fig. 7). As indicated above, the average distances that separate C-2, C-3 and C-4 of biphenyl from the Fe of BphAE_{LB400} are respectively 4 Å, 4 Å and 5 Å. The fact that C-2/C-3/C-4 of 2,6-dichlorobiphenyl are instead at similar distances from the Fe atom of BphAE_{p4} may explain why BphAE_{p4} produced a large amount of the 3,4-dihydro-dihydroxy metabolite from 2,6-dichlorobiphenyl.

The corresponding atoms of both substrates interact with the same residues of BphAE_{p4} and BphAE_{LB400} α subunits (Leu333, Phe227, Gln226, His323, His233, Ala230, Met231) and they are located at similar distances (closer than 4.5 Å) (Supplementary material Fig. 3c). Most residues that were closer than 4.5 Å from the distal ring in BphAE_{LB400} (Phe384, His239, Phe336, Met231, Gly321, Val287) are at a similar distance from the non-reactive ring of 2,6-dichlorobiphenyl in BphAE_{p4} (supplementary material Fig. 3d). As noted above, relative to the BphAE_{LB400}:biphenyl complex, the non-reactive ring of 2,6-dichlorobiphenyl shifts toward the Val320-Gln322 segment and Met336. As shown in Fig. 5, the Val320-Gln322 segment of BphAE_{p4} assumes various conformations in the absence of substrate, indicating it is less constrained in BphAE_{p4} than in BphAE_{LB400}. This allows displacement on the order of 2 Å during binding to 2,6-dichlorobiphenyl, generating space for the *ortho* chlorine. This adjustment did not change the cavity volume of BphAE_{p4} as the average cavity volume of the $\alpha\beta$ dimers of the native enzyme (as calculated using CASTp program)

was 1152 Å³ and the average value for dimers GH, IJ, KL of the complexed enzyme was 1159 Å³.

In addition, relative to BphAE_{LB400} the BphAE_{p4} 280–283 segment shows more variation in conformation in the absence of substrate, and this segment clearly shifts by 1 to 2 Å toward the substrate when BphAE_{p4} binds 2,6-dichlorobiphenyl (Fig.5). Altogether, either because it is larger than biphenyl or as a result of interaction between the two *ortho*-chlorine atoms of the non-reactive ring with residues lining the distal catalytic pocket, binding of 2,6-dichlorobiphenyl requires or induces more conformational changes than biphenyl binding. The fact that BphAE_{LB400} poorly catalyzes the oxygenation of 2,6-dichlorobiphenyl suggests that in spite of the large size of its catalytic pocket, the space available near the *ortho*-chlorines is not sufficient to allow productive binding of this substrate. In fact, automated docking of 2,6-dichlorobiphenyl into BphAE_{LB400} places the non-chlorinated ring into the distal pocket of the enzyme and the chlorinated ring into the proximal pocket. In such "flipped" structures, neither the C-2'/C-3' nor C-3'/C-4' carbons of the chlorinated ring align with C-2/C-3 of the BphAE_{LB400}:biphenyl complex, and they are very far from the iron atom (not shown).

Aside from the segments comprising residues Glu280-Ser283 and Val320-Glu322 and of residue Asp388, other segments or residues of the α subunit including Tyr277-Val278, Lys403-Ala411, Gly427-Tyr433, His233-His239 are displaced after BphAE_{p4} binds to 2,6-dichlorobiphenyl (not shown). However, the possible impact of these movements on the catalytic activity toward 2,6-dichlorobiphenyl is not as readily explained.

Effect of the Thr335-to-Ala mutation

Analysis of the crystal structures of BphAE_{p4} and BphAE_{LB400} suggests how changing Thr335 to Ala alters the conformational freedom of the Val320-Gly321 segment and some of the other segments of the catalytic pocket. In BphAE_{LB400}, the hydroxyl group of Thr335 is within 3.0 Å of the amide groups of Gln322 and of Gly321 and within 3.5 Å of C-1 of Val320. In addition, hydrogen bonds are formed between the amide groups of Gly321 and Gln322 and the hydroxyl group of Thr335. Most of these contacts are lost when Thr335 is replaced by Ala (Fig. 8). This appears to relax conformational constraints for the Val320-Gln322 segment, which allows for greater variation in conformation and displacement of this segment, particularly for the carbonyl group of Gly321. Replacing Thr335 by Ala has other consequences for residues lining the catalytic cavity. Since Gly321 and Val320 form hydrogen bonds with Tyr277, the conformation of the Val320-Gln322 segment influences the conformation of this residue. In addition, although residues Arg318-Met319 do not contact Thr335, their conformation appears to be influenced by the position and orientation of 320–322. Moreover, residues 320–322 can influence indirectly the conformation of the Asn279-Ser283 segment through contacts between the latter and Arg318-Met319 (Fig. 8). Thus the considerable shift of Ser283 and Glu280 after substrate binding can be linked back to the relaxation of conformational restraints for Val320-Gln322. Another consequence of this movement is to close the mouth of the active site, but it is not clear if this shift is required for productive binding of 2,6-dichlorobiphenyl.

Discussion

Examination of the substrate binding interactions and the structural mechanism by which BPDOs can increase their metabolic versatility will advance approaches to engineer better performing biocatalysts. Many investigations have shown that the specificities and regiospecificities of Rieske-type aryl hydroxylating dioxygenases were altered by changing single residues that crystal structures place near the active site^{22; 30; 31}. These studies and many others involving other enzymes^{30; 31; 32; 33; 34; 35; 36}, have demonstrated that these

changes can alter the configuration of the space within the catalytic pocket. In the case of versatile enzymes such as aryl hydroxylating dioxygenases and cytochromes P450, many of which can oxygenate a broad range of substrates, induced-fit mechanisms are likely to be required to allow productive substrate binding. One mechanism to enhance the capacity for induced-fit is to lessen the structural constraints imposed on strategic active site residues. Residues lining the catalytic cavity that are less constrained are able to change conformation during substrate binding allowing more space for productive binding of structurally different substrates. Hence changes induced by substrate binding have been observed for several cytochromes P450³⁷. Similarly, in the case of Rieske-type oxygenases, crystallographic studies of NDO³⁸, nitrotoluene dioxygenase³⁹, BphA1A2_{RHA1}¹⁸ as well as BphA1A2_{B1}²⁴ and BphAE_{p4} showed that some of the residues lining the distal and also the proximal portion of the catalytic pocket can be displaced by substrate binding. Here, structural analysis of native and substrate-bound BphAE_{LB400} and BphAE_{p4} revealed conformational variations of the carbonyl group of Gly321, which is in direct, non-bonded contact with substrates. The corresponding residue in BphA1A2_{RHA1} was also shown to be displaced after substrate binding¹⁸. Our data also reveal how other residues not in direct contact with the substrate, such as Ala335 of BphAE_{p4}, can influence the adaptability of the catalytic pocket of BPDO and thereby allow productive substrate binding. Thus, changing Thr335 to Ala relaxed constraints on the Val320-Gly321-Gln322 segment allowing displacement of Gly321 during substrate binding and opening space to position and orient the doubly-*ortho*-chlorinated biphenyl inside the catalytic pocket.

Although Thr335 appears to play a controlling role in the inability of BphAE_{LB400} to oxygenate 2,6-dichlorobiphenyl, the identity of residue 336 also has significant influence on the reaction because BphAE_{p4} and BphAE_{p401} have different regiospecificity toward this substrate. The structures suggest differences in side chain interactions between Phe336 or Met336 and the distal ring influence the relationship of the reactive ring relative to the Fe. It is noteworthy that the distances from C-2/C-3 to the Fe atom are significantly larger in the BphAE_{p4}:2,6-dichlorobiphenyl complex compared to the distances in the BphAE_{LB400}:biphenyl complex. In addition, in the BphAE_{p4}:2,6-dichlorobiphenyl complex, the C-2 and C-4 carbons are equidistant from the Fe, which may readily explain the enhanced yield of the 3,4-hydroxylated product in Met336 variants. Similarly, Phe336 and Met336 probably interact differently with 2,2'-dichlorobiphenyl since the regiospecificity toward this substrate is changed when Phe336 of BphAE_{LB400} is replaced by Met in BphAE_{p402} and BphAE_{p4}.

It is also noteworthy that BphAE_{B-356} and variant BphAE_{II9}, which was obtained by replacing residues 335–341 of BphAE_{LB400} by the corresponding residues of BphAE_{B-356}, can oxygenate 2,6-dichlorobiphenyl¹⁶. In this case, Thr335-Phe336 of BphA_{LB400} are replaced by Gly-Ile, and it is most likely that, similar to BphAE_{p4}, the replacement of Thr335 by a Gly reduces constraints on residues 320–322 to facilitate the movement of Gly321. However, BphAE_{B-356} and BphAE_{II9}, both produce principally the 2,3-dihydro-2,3-dihydroxy-dichlorobiphenyl from 2,6-dichlorobiphenyl. This suggests that Met336 of BphAE_{p4} and the corresponding residue of BphAE_{B-356}, Thr333, interact differently with the substrate to influence its orientation inside the catalytic cavity. This would not be surprising given the differences in the chemistry and conformation variations of Met and Thr residues.

We recently examined the diversity of the BphA C-terminal domain as represented by PCR products amplified from various PCB degrading bacteria and from DNA extracted from PCB-contaminated soils. The presence of a Thr at position 335 as in BphA_{LB400} was uncommon, and most of the sequences contained the smaller Gly or Ala at that position⁴⁰. This leads to the hypothesis that, in most BphAs, the Val320-Gln322 segment is more

relaxed than in BphA_{LB400}. To our knowledge, no study has examined the effect of replacing Gly321 with larger amino acids in the background of BphA_{LB400}, but additional recent observations emphasized the importance of residue 321 as a determinant for substrate specificity^{40; 41}. Thus, Witzig et al.⁴¹ amplified the C-terminal portion of genes encoding the α subunit of toluene/biphenyl dioxygenases from isolates growing on benzene-toluene-ethylbenzene and from soil DNA from which they were isolated. The position corresponding to Gly321 was highly variable. However, the isolates harboring a bulkier amino acid at that position were unable to oxygenate toluene⁴¹.

Other residues that line the catalytic cavity were previously found to influence the substrate specificity and regioselectivity. Suenaga et al.²² found that changing Phe227, Leu333, Phe377 and Phe383 of *Pseudomonas pseudoalcaligenes* KF707 BphA1 (BphA1_{KF707}), corresponding to Phe227, Leu333, Phe378 and Phe384 of BphA_{LB400}, alter either the range of substrates that the enzyme can oxygenate or the regioselectivity toward *ortho*-chlorinated biphenyls. Both a homology model of BphA1_{KF707} based on BphA1_{RHA1}, and our crystal structures of BphA_{LB400} show that these residues line the catalytic pocket and thus may critically influence the enzyme's catalytic properties toward chlorobiphenyls. However, Zielinski et al.²³ and Vézina et al.⁴² identified other residues that are not expected to be in direct contact with the substrate but significantly modified the specificities and/or regioselectivities toward selected substrates. Perhaps some of these residues influence the catalytic properties indirectly by controlling the position and/or conformation of residues lining the catalytic cavity or by altering the level of constraint imposed on protein segments lining the catalytic cavity to allow more movement during substrate binding. The case of Asn377 is of particular interest since the variant obtained by replacing the corresponding Thr376 of BphA1_{KF707} by Asn of BphA_{LB400} has acquired the ability to oxygenate 2,2', 5,5'-tetrachlorobiphenyl onto carbon atoms 3 and 4⁴³. An analysis³¹ based on a homology model of BphA1_{KF707} suggested that the loss of a hydrogen bond involving the hydroxyl residue of Thr376 with the carbonyl of Asn373 could be responsible for the different regioselectivities between wild-type BphA1_{KF707} and its Thr376Asn variant. However, in the absence of crystal structures of BphA1A2_{KF707} and the variant, the authors were unable to explain how the loss of this hydrogen bond influenced the catalytic properties of the enzyme. Since Phe378 (Phe377 of BphA1_{KF707}) is close to carbon 3 and 4 of biphenyl's distal ring, it is possible that relaxation of constraints on residues 376–377 of BphA1_{KF707}, associated with loss of the hydrogen bond, allows an adaptive response centered on Phe377 that creates more space to accept and position the doubly *ortho-meta* tetrachlorinated congener.

The results obtained in this work increase our understanding of how amino acid residues within and outside the active site pocket can affect substrate specificity and enzyme activity. Data show how the mutations directed at residues further removed from the substrate can influence the enzyme's specificities. Consistent with induced-fit mechanisms, these mutations can modulate the spatial distribution of residues in direct contact with the substrate or influence the binding-induced changes required to place chlorobiphenyls into productive positions and orientations. Additional effort will be required to determine the precise mechanisms by which additional residues not in direct contact with the substrate influence the enzyme's specificities. At a fundamental level, our results plead in favor of engineering aryl hydroxylating enzymes through artificial evolutionary approaches that alter all or specific protein segments in the vicinity of the catalytic cavity instead of changing individual residues that are in direct contact with the substrate.

Materials and Methods

Strains, plasmids and chemicals

E. coli DH11S⁴⁴ and C41(DE3)⁴⁵ (Statagene, La Jolla, CA) were used in this study. The plasmids used were pT76a⁴⁶, pET14b[*p4-bphAE*] and pET14b[LB400-*bphAE*]⁴⁷ and pQE31[LB400-*bphAE*] and pQE31[*p4-bphAE*]¹⁵. Biphenyl and the chlorobiphenyls used in this work were of the highest purity grade available from AccuStandard (New Haven, CT).

Mutagenesis and cloning

The mutated genes for variants BphAE_{p401} (T335A) and variant BphAE_{p402} (F336M) were prepared from LB400 *bphAE* by the two-step site-directed mutagenesis protocol described previously,⁴² creating pQE31[LB400-*bphAE*_{p401}] and pQE31[LB400-*bphAE*_{p402}]. The resulting plasmids were transformed into *E. coli* DH11S pDB31[LB400-*bphFG*]¹⁴. DNA protocols were generally according to Sambrook et al.⁴⁸. DNA from each mutant was sequenced at the Génome Québec DNA Sequencing Center (Montreal, Quebec, Canada).

Whole cell assays to identify metabolites of chlorobiphenyls

Metabolites were analyzed from suspensions of isopropyl β -D-1-thiogalactopyranoside (IPTG)-induced *E. coli* DH11S pDB31[LB400-*bphFG*] harboring appropriate variants of pQE31[*bphAE*] according to the protocol described previously¹⁵. Level of expression was assessed by inspection of SDS-PAGE gels⁴⁹. Metabolites were identified by gas chromatography-mass spectrometry (GC-MS) analyses of their butylboronate derivatives¹⁵. GC-MS peak areas were used to determine the relative activity of each variant enzyme.

Crystallization and crystallographic methods

Purification, crystallization, and preliminary X-ray diffraction properties of BphAE_{LB400} and BphAE_{p4} have been communicated elsewhere (Kumar *et al.*, submitted). In brief, crystallization conditions for BphAE_{LB400} and BphAE_{p4} were screened by the sitting-drop vapor-diffusion method at 21°C under an N₂ atmosphere (<5 ppm oxygen) in a glove box (Innovative Technologies, Newburyport, MA). BphAE_{LB400} crystals grew in triclinic space group *P*1 with twelve $\alpha\beta$ dimers (i.e., four $\alpha_3\beta_3$ hexamers) in the asymmetric unit at 21°C when the reservoir solution (1000 μ l) contained 20–25% (w/v) PEG 8000 or PEG 5000 MME, 50 mM PIPES pH 6.5, 100 mM ammonium acetate, 5% (v/v) glycerol and 0.2% (w/v) agarose. BphAE_{p4} grew in two different crystal forms at 21°C using a reservoir solution (1000 μ l) containing 20–25% (w/v) PEG 8000, 50 mM PIPES pH 6.5 and 100 mM ammonium acetate. Absent substrate, BphAE_{p4} enzyme crystallized in triclinic space group *P*1 with twelve $\alpha\beta$ dimers in the asymmetric unit, whereas crystals of the BphAE_{p4}:2,6-dichlorobiphenyl complex have monoclinic space group *P*2₁, with six $\alpha\beta$ dimers in the asymmetric unit.

Diffraction data were acquired from cryogenically cooled crystals (100K) using the facilities of SERCAT beamline 22-ID at the Advanced Photon Source (Argonne National Laboratories). The diffraction patterns were indexed, integrated and scaled using the *HKL2000* suite⁵⁰. Initial phases for BphAE_{LB400} and BphAE_{p4} were obtained by the molecular replacement method using MOLREP⁵¹ from the *CCP4* v.4.2 software suite⁵². In case of BphAE_{LB400}, the crystal structure of BphAE_{B356}¹⁶ was used as the search model. Atomic model refinement was accomplished using the program CNS⁵³ and REFMAC5.2⁵⁴. The programs O⁵⁵ and COOT⁵⁶ were used for analysis of electron density maps and model building. Stereochemical properties of models were evaluated using Procheck⁵⁷ and Ramachandran plots. Several cycles of rigid body refinement and then restrained refinement were used to achieve acceptable R_{cryst} and R_{free} . The CASTp program²⁷ which was available

online (<http://sts.bioengr.uic.edu/castp/index.php>) was used to calculate the catalytic cavity volume using a probe radius of 1.4Å. Figures were prepared using the program PyMOL.

PDB accession codes

The coordinates have been deposited with the RCSB Protein Data Bank (<http://deposit.rcsb.org/>) under accession codes 2xr8 for BphAE_{LB400} and 2xrx for its biphenyl-complex form and 2xso for BphAE_{p4} and 2xsh for its complex with 2,6-dichlorobiphenyl.

Supplementary Material

Refer to Web version on PubMed Central for supplementary material.

Acknowledgments

This work was supported by Discovery and Strategic grants from the Natural Sciences and Engineering Research Council of Canada (NSERC). Use of the BioCARS Sector 14 at the Advanced Photon Source (APS), Argonne National Laboratory, was supported by the National Institutes of Health, National Center for Research Resources, under grant number RR007707. Additional X-ray diffraction data were collected at APS using Southeast Regional Collaborative Access Team (SER-CAT) 22-ID beamline; supporting institutions may be found at www.ser-cat.org/members.html. Use of the Advanced Photon Source was supported by the U. S. Department of Energy, Office of Science, Office of Basic Energy Sciences, under Contract No. W-31-109-Eng-38.

References

1. Aoki Y. Polychlorinated biphenyls, polychlorinated dibenzo-p-dioxins, and polychlorinated dibenzofurans as endocrine disrupters--what we have learned from Yusho disease. *Environ Res.* 2001; 86:2–11. [PubMed: 11386736]
2. Safe SH. Polychlorinated biphenyls (PCBs) - Environmental impact, biochemical and toxic responses, and implications for risk assessment. *Crit Rev Toxicol.* 1994; 24:87–149. [PubMed: 8037844]
3. Misawa N, Nakamura R, Kagiya Y, Ikenaga H, Furukawa K, Shindo K. Synthesis of vicinal diols from various arenes with a heterocyclic, amino or carboxyl group by using recombinant *Escherichia coli* cells expressing evolved biphenyl dioxygenase and dihydrodiol dehydrogenase genes. *Tetrahedron.* 2005; 61:195–204.
4. Resnick SM, Gibson DT. Regio- and stereospecific oxidation of fluorene, dibenzofuran, and dibenzothiophene by naphthalene dioxygenase from *Pseudomonas* sp strain NCIB 9816-4. *Appl Environ Microbiol.* 1996; 62:4073–4080. [PubMed: 8899998]
5. Seeger M, Gonzalez M, Camara B, Munoz L, Ponce E, Mejias L, Mascayano C, Vasquez Y, Sepulveda-Boza S. Biotransformation of natural and synthetic isoflavonoids by two recombinant microbial enzymes. *Appl Environ Microbiol.* 2003; 69:5045–5050. [PubMed: 12957885]
6. Ullrich R, Hofrichter M. Enzymatic hydroxylation of aromatic compounds. *Cell Mol Life Sci.* 2007; 64:271–293. [PubMed: 17221166]
7. Erickson BD, Mondello FJ. Nucleotide sequencing and transcriptional mapping of the genes encoding biphenyl dioxygenase, a multicomponent polychlorinated-biphenyl-degrading enzyme in *Pseudomonas* strain LB400. *J Bacteriol.* 1992; 174:2903–2912. [PubMed: 1569021]
8. Hurtubise Y, Barriault D, Sylvestre M. Characterization of active recombinant his-tagged oxygenase component of *Comamonas testosteroni* B-356 biphenyl dioxygenase. *J Biol Chem.* 1996; 271:8152–8156. [PubMed: 8626504]
9. Karlsson A, Parales JV, Parales RE, Gibson DT, Eklund H, Ramaswamy S. Crystal structure of naphthalene dioxygenase: Side-on binding of dioxygen to iron. *Science.* 2003; 299:1039–1042. [PubMed: 12586937]
10. Mondello FJ, Turcich MP, Lobos JH, Erickson BD. Identification and modification of biphenyl dioxygenase sequences that determine the specificity of polychlorinated biphenyl degradation. *Appl Environ Microbiol.* 1997; 63:3096–3103. [PubMed: 9251195]

11. Maltseva OV, Tsoi TV, Quensen JF, Fukuda M, Tiedje JM. Degradation of anaerobic reductive dechlorination products of Aroclor 1242 by four aerobic bacteria. *Biodegradation*. 1999; 10:363–371. [PubMed: 10870552]
12. Rodrigues JLM, Kachel CA, Aiello MR, Quensen JF, Maltseva OV, Tsoi TV, Tiedje JM. Degradation of Aroclor 1242 dechlorination products in sediments by *Burkholderia xenovorans* LB400(Ohb) and *Rhodococcus* sp strain RHA1(Fcb). *Appl Environ Microbiol*. 2006; 72:2476–2482. [PubMed: 16597946]
13. Furukawa K, Tonomura K, Kamibayashi A. Effect of chlorine substitution on the biodegradability of polychlorinated biphenyls. *Appl Environ Microbiol*. 1978; 35:223–227. [PubMed: 16345265]
14. Barriault D, Plante MM, Sylvestre M. Family shuffling of a targeted *bphA* region to engineer biphenyl dioxygenase. *J Bacteriol*. 2002; 184:3794–3800. [PubMed: 12081948]
15. Barriault D, Sylvestre M. Evolution of the biphenyl dioxygenase BphA from *Burkholderia xenovorans* LB400 by random mutagenesis of multiple sites in region III. *J Biol Chem*. 2004; 279:47480–47488. [PubMed: 15342624]
16. Gomez-Gil L, Kumar P, Barriault D, Bolin JT, Sylvestre M, Eltis LD. Characterization of biphenyl dioxygenase of *Pandoraea pnomenus* B-356 as a potent polychlorinated biphenyl-degrading enzyme. *J Bacteriol*. 2007; 189:5705–5715. [PubMed: 17526697]
17. Dong XS, Fushinobu S, Fukuda E, Terada T, Nakamura S, Shimizu K, Nojiri H, Omori T, Shoun H, Wakagi T. Crystal structure of the terminal oxygenase component of cumene dioxygenase from *Pseudomonas fluorescens* IP01. *J Bacteriol*. 2005; 187:2483–2490. [PubMed: 15774891]
18. Furusawa Y, Nagarajan V, Tanokura M, Masai E, Fukuda M, Senda T. Crystal structure of the terminal oxygenase component of biphenyl dioxygenase derived from *Rhodococcus* sp. strain RHA1. *J Mol Biol*. 2004; 342:1041–1052. [PubMed: 15342255]
19. Friemann R, Lee K, Brown EN, Gibson DT, Eklund H, Ramaswamy S. Structures of the multicomponent Rieske non-heme iron toluene 2,3-dioxygenase enzyme system. *Acta Crystallogr D Biol Crystallogr*. 2009; 65:24–33. [PubMed: 19153463]
20. Yu CL, Liu W, Ferraro DJ, Brown EN, Parales JV, Ramaswamy S, Zylstra GJ, Gibson DT, Parales RE. Purification, characterization, and crystallization of the components of a biphenyl dioxygenase system from *Sphingobium yanoikuyae* B1. *J Ind Microbiol Biot*. 2007; 34:311–324.
21. Suenaga H, Goto M, Furukawa K. Emergence of multifunctional oxygenase activities by random priming recombination. *J Biol Chem*. 2001; 276:22500–22506. [PubMed: 11312272]
22. Suenaga H, Watanabe T, Sato M, Ngadiman, Furukawa K. Alteration of regiospecificity in biphenyl dioxygenase by active-site engineering. *J Bacteriol*. 2002; 184:3682–3688. [PubMed: 12057964]
23. Zielinski M, Kahl S, Hecht HJ, Hofer B. Pinpointing biphenyl dioxygenase residues that are crucial for substrate interaction. *J Bacteriol*. 2003; 185:6976–6980. [PubMed: 14617661]
24. Ferraro DJ, Brown EN, Yu CL, Parales RE, Gibson DT, Ramaswamy S. Structural investigations of the ferredoxin and terminal oxygenase components of the biphenyl 2,3-dioxygenase from *Sphingobium yanoikuyae* B1. *BMC Struct Biol*. 2007; 7:10. [PubMed: 17349044]
25. Jakoncic J, Jouanneau Y, Meyer C, Stojanoff V. The crystal structure of the ring-hydroxylating dioxygenase from *Sphingomonas* CHY-1. *FEBS Journal*. 2007; 274:2470–2481. [PubMed: 17451434]
26. Kauppi B, Lee K, Carredano E, Parales RE, Gibson DT, Eklund H, Ramaswamy S. Structure of an aromatic-ring-hydroxylating dioxygenase-naphthalene 1,2-dioxygenase. *Structure*. 1998; 6:571–586. [PubMed: 9634695]
27. Dundas J, Ouyang Z, Tseng J, Binkowski A, Turpaz Y, Liang J. CASTp: computed atlas of surface topography of proteins with structural and topographical mapping of functionally annotated residues. *Nucleic Acids Res*. 2006; 34:W116–W118. [PubMed: 16844972]
28. Hurtubise Y, Barriault D, Sylvestre M. Involvement of the terminal oxygenase *beta* subunit in the biphenyl dioxygenase reactivity pattern toward chlorobiphenyls. *J Bacteriol*. 1998; 180:5828–5835. [PubMed: 9811638]
29. Hirose J, Suyama A, Hayashida S, Furukawa K. Construction of hybrid biphenyl (*bph*) and toluene (*tod*) genes for functional analysis of aromatic ring dioxygenases. *Gene*. 1994; 138:27–33. [PubMed: 8125315]

30. Parales RE, Lee K, Resnick SM, Jiang HY, Lessner DJ, Gibson DT. Substrate specificity of naphthalene dioxygenase: Effect of specific amino acids at the active site of the enzyme. *J Bacteriol.* 2000; 182:1641–1649. [PubMed: 10692370]
31. Suenaga H, Goto M, Furukawa K. Active-site engineering of biphenyl dioxygenase: effect of substituted amino acids on substrate specificity and regioselectivity. *Appl Microbiol Biotechnol.* 2006; 71:168–176. [PubMed: 16217654]
32. Bak-Jensen KS, Andre G, Gottschalk TE, Paes G, Tran V, Svensson B. Tyrosine 105 and threonine 212 at outermost substrate binding subsites –6 and +4 control substrate specificity, oligosaccharide cleavage patterns, and multiple binding modes of barley alpha-amylase 1. *J Biol Chem.* 2004; 279:10093–10102. [PubMed: 14660599]
33. Dietrich M, Do TA, Schmid RD, Pleiss J, Urlacher VB. Altering the regioselectivity of the subterminal fatty acid hydroxylase P450 BM-3 towards *gamma*- and *delta*-positions. *J Biotechnol.* 2009; 139:115–117. [PubMed: 18984016]
34. Huang WC, Westlake AC, Marechal JD, Joyce MG, Moody PC, Roberts GC. Filling a hole in cytochrome P450 BM3 improves substrate binding and catalytic efficiency. *J Mol Biol.* 2007; 373:633–651. [PubMed: 17868686]
35. Ostrander EL, Larson JD, Schuermann JP, Tanner JJ. A conserved active site tyrosine residue of proline dehydrogenase helps enforce the preference for proline over hydroxyproline as the substrate. *Biochemistry.* 2009; 48:951–959. [PubMed: 19140736]
36. Xu D, Enroth C, Lindqvist Y, Ballou DP, Massey V. Studies of the mechanism of phenol hydroxylase: effect of mutation of proline 364 to serine. *Biochemistry.* 2002; 41:13627–13636. [PubMed: 12427024]
37. Isin EM, Guengerich FP. Substrate binding to cytochromes P450. *Anal Bioanal Chem.* 2008; 392:1019–1030. [PubMed: 18622598]
38. Carredano E, Karlsson A, Kauppi B, Choudhury D, Parales RE, Parales JV, Lee K, Gibson DT, Eklund H, Ramaswamy S. Substrate binding site of naphthalene 1,2-dioxygenase: Functional implications of indole binding. *J Mol Biol.* 2000; 296:701–712. [PubMed: 10669618]
39. Friemann R, IvkovicJensen MM, Lessner DJ, Yu CL, Gibson DT, Parales RE, Eklund H, Ramaswamy S. Structural insight into the dioxygenation of nitroarene compounds: the crystal structure of nitrobenzene dioxygenase. *J Mol Biol.* 2005; 348:1139–1151. [PubMed: 15854650]
40. Vézina J, Barriault D, Sylvestre M. Diversity of the C-terminal portion of the biphenyl dioxygenase large subunit. *J Mol Microb Biotech.* 2008; 15:139–151.
41. Witzig R, Junca H, Hecht HJ, Pieper DH. Assessment of toluene/biphenyl dioxygenase gene diversity in benzene-polluted soils: links between benzene biodegradation and genes similar to those encoding isopropylbenzene dioxygenases. *Appl Environ Microbiol.* 2006; 72:3504–3514. [PubMed: 16672497]
42. Vézina J, Barriault D, Sylvestre M. Family shuffling of soil DNA to change the regioselectivity of *Burkholderia xenovorans* LB400 biphenyl dioxygenase. *J Bacteriol.* 2007; 189:779–788. [PubMed: 17142386]
43. Suenaga H, Nishi A, Watanabe T, Sakai M, Furukawa K. Engineering a hybrid pseudomonad to acquire 3,4-dioxygenase activity for polychlorinated biphenyls. *J Biosci Bioeng.* 1999; 87:430–435. [PubMed: 16232495]
44. Lin JJ, Smith M, Jessee J, Bloom F. DH11s: an *E. coli* strain for preparation of single-stranded DNA from phagemid vectors. *BioTechniques.* 1992; 12:718–721. [PubMed: 1515139]
45. Miroux B, Walker JE. Over-production of proteins in *Escherichia coli*: mutant hosts that allow synthesis of some membrane proteins and globular proteins at high levels. *J Mol Biol.* 1996; 260:289–298. [PubMed: 8757792]
46. Hofer B, Eltis LD, Dowling DN, Timmis KN. Genetic analysis of a *Pseudomonas* locus encoding a pathway for biphenyl/polychlorinated biphenyl degradation. *Gene.* 1993; 130:47–55. [PubMed: 8344527]
47. Mohammadi M, Sylvestre M. Resolving the profile of metabolites generated during oxidation of dibenzofuran and chlorodibenzofurans by the biphenyl catabolic pathway enzymes. *Chem Biol.* 2005; 12:835–846. [PubMed: 16039530]

48. Sambrook, J.; Fritsch, EF.; Maniatis, T. *Molecular cloning: a laboratory manual*. Cold Spring Harbor, NY: Spring Harbor Laboratory Press; 1989.
49. Laemmli CM, Leveau JH, Zehnder AJ, van der Meer JR. Characterization of a second *tfd* gene cluster for chlorophenol and chlorocatechol metabolism on plasmid pJP4 in *Ralstonia eutropha* JMP134(pJP4). *J Bacteriol*. 2000; 182:4165–4172. [PubMed: 10894723]
50. Otwinowski Z, Minor W. Processing of X-ray diffraction data collected in oscillation mode. *Method Enzymol*. 1997; 276:307–326.
51. Vagin A, Teplyakov A. MOLREP: an automated program for molecular replacement. *J Appl Crystallogr*. 1997; 30:1022–1025.
52. COLLABORATIVE, COMPUTATIONAL & PROJECT. The CCP4 suite: programs for protein crystallography. *Acta Crystallogr D Biol Crystallogr*. 1994; 50:760–763. [PubMed: 15299374]
53. Brünger AT, Adams PD, Clore GM, DeLano WL, Gros P, Grosse-Kunstleve RW, Jiang JS, Kuszewski J, Nilges M, Pannu NS, Read RJ, Rice LM, Simonson T, Warren GL. Crystallography & NMR system: A new software suite for macromolecular structure determination. *Acta Crystallogr D Biol Crystallogr*. 1998; 54:905–921. [PubMed: 9757107]
54. Murshudov GN, Vagin AA, Dodson EJ. Refinement of macromolecular structures by the maximum-likelihood method. *Acta Crystallogr D Biol Crystallogr*. 1997; 53:240–255. [PubMed: 15299926]
55. Jones TA, Zou JY, Cowan SW, Kjeldgaard M. Improved methods for building protein models in electron-density maps and the location of errors in these models. *Acta Crystallogr A*. 1991; 47:110–119. [PubMed: 2025413]
56. Emsley P, Cowtan K. Coot: model-building tools for molecular graphics. *Acta Crystallogr D Biol Crystallogr*. 2004; 60:2126–2132. [PubMed: 15572765]
57. Laskowski RA, Macarthur MW, Moss DS, Thornton JM. Procheck - a program to check the stereochemical quality of protein structures. *J Appl Crystallogr*. 1993; 26:283–291.

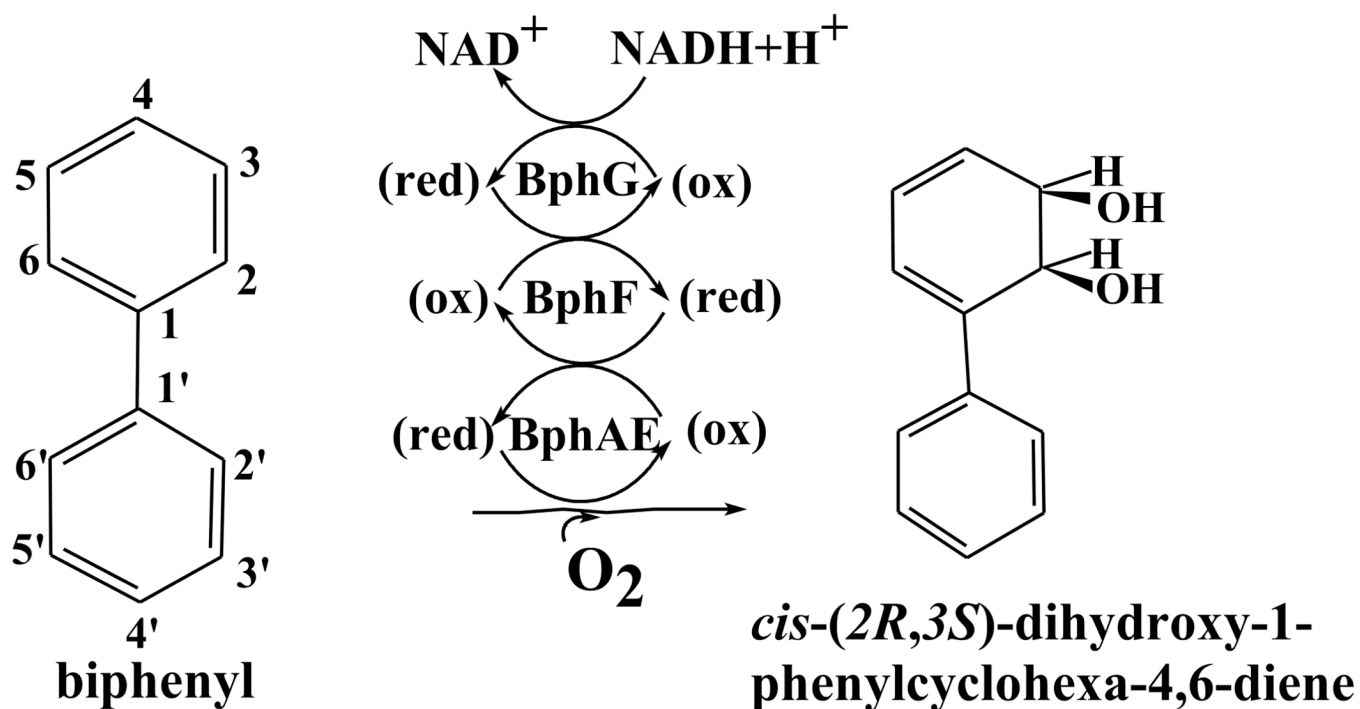


Figure 1.
The BPDO components and encoding genes in *B. xenovorans* LB400.

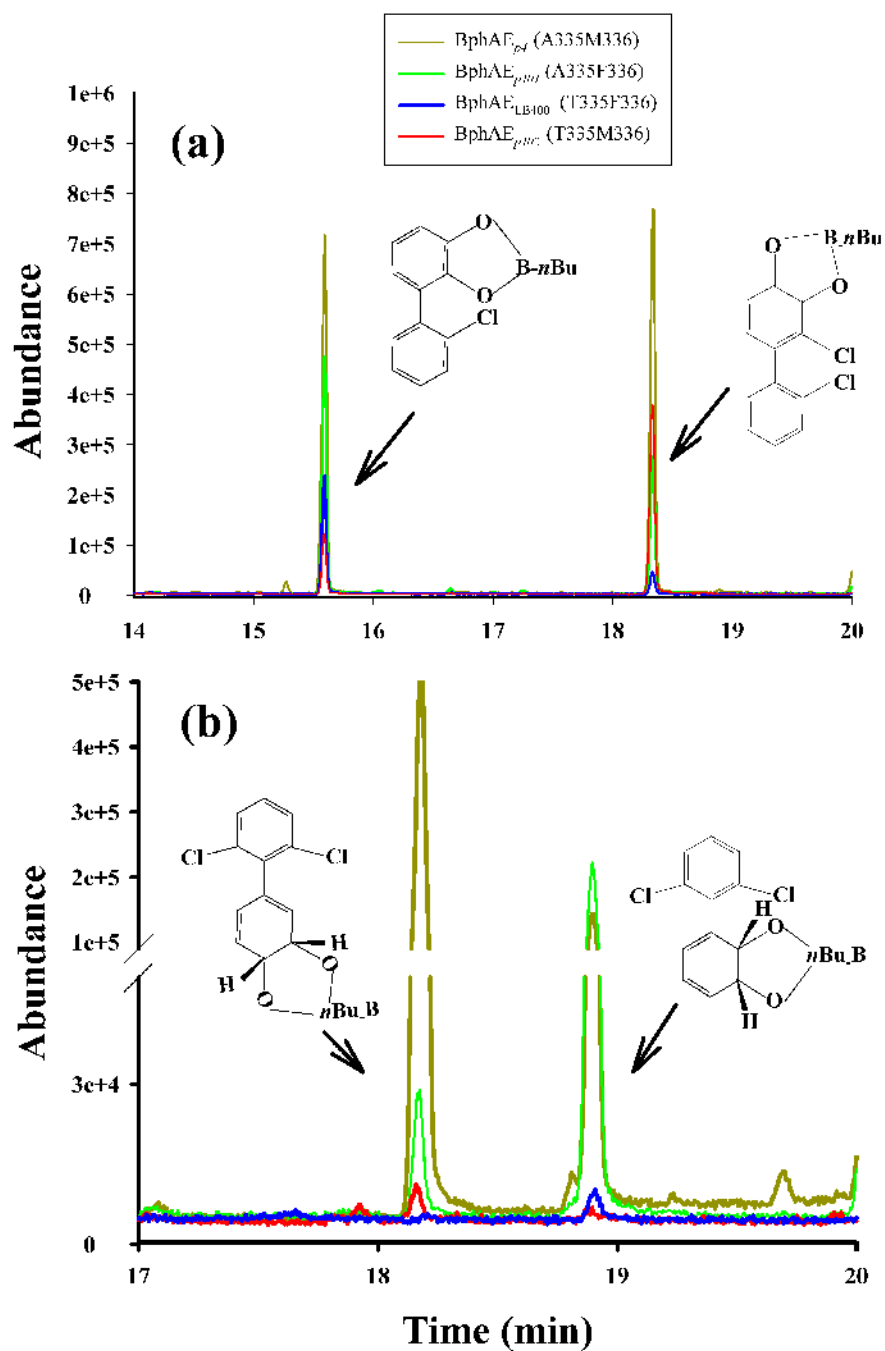


Figure 2. GC-MS spectra of butylboronate-derived metabolites produced (a) from 2,2'-dichlorobiphenyl and (b) from 2,6-dichlorobiphenyl by BphAE_{LB400} and its variants.

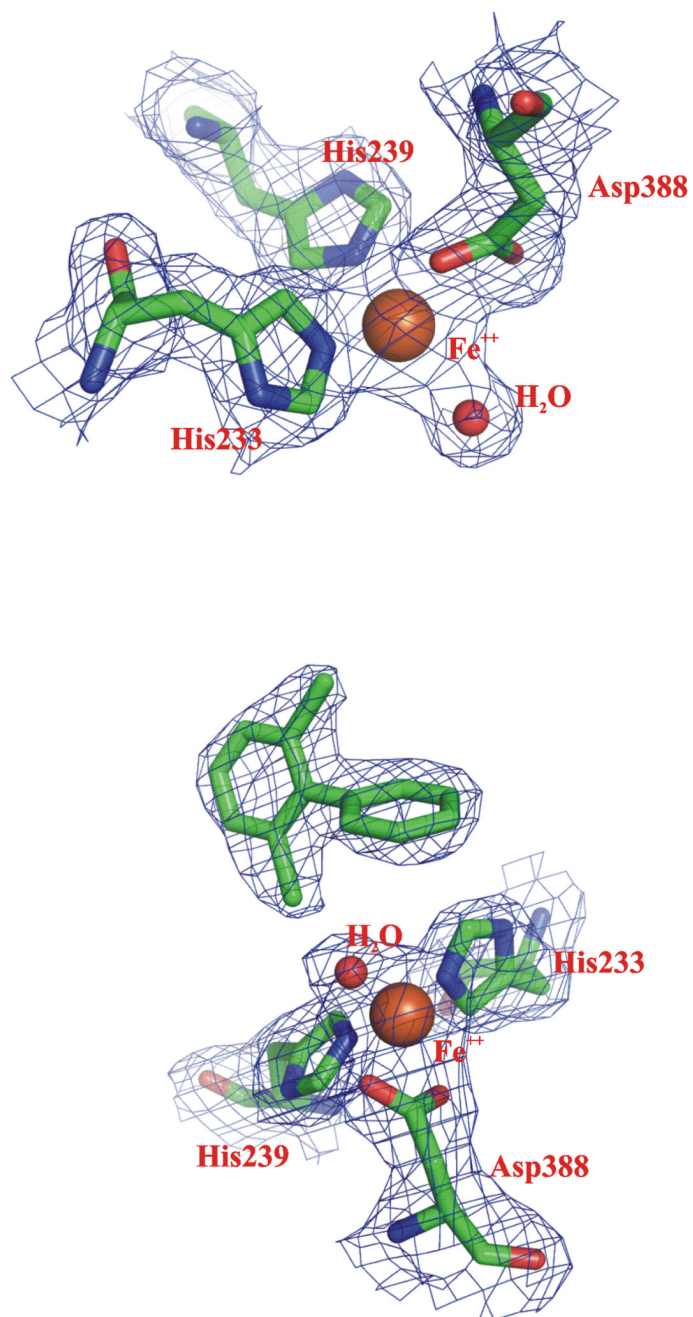


Fig. 4. The $2F_{obs} - F_{calc}$ electron density map of chain AB of substrate-free (upper panel) and of 2,6-dichlorobiphenyl-complex (lower panel) of BphAE_{p4} contoured at 1.0 σ level.

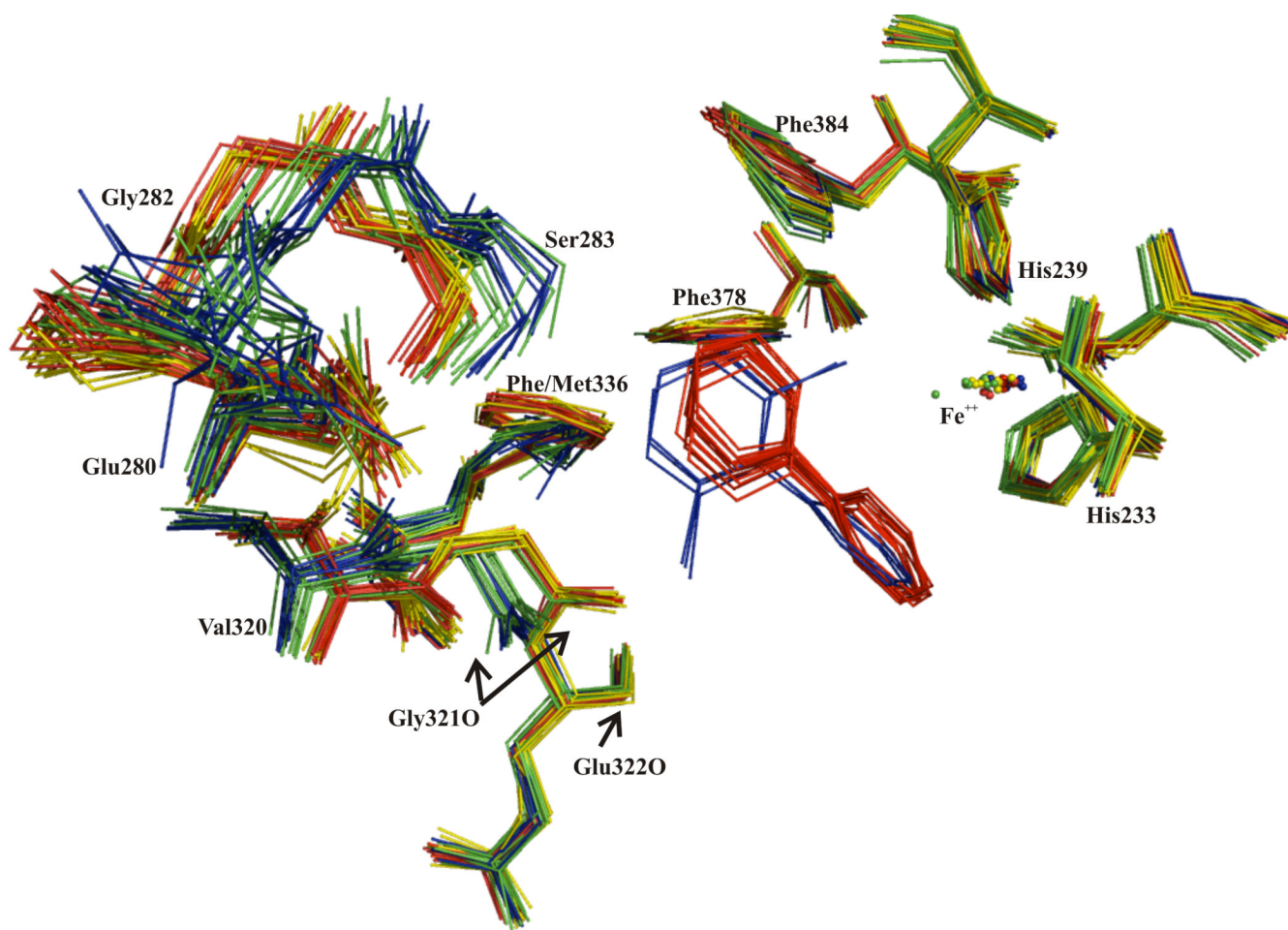


Figure 5. Superposition of active site atoms from twelve $\alpha\beta$ dimers of BphAE_{LB400} (yellow) and twelve biphenyl-bound dimers (red) with twelve $\alpha\beta$ dimers of BphAE_{p4} (green) and six dimers of 2,6-dichlorobiphenyl-bound BphAE_{p4} (blue) showing the shift of the distal ring of 2,6-dichlorobiphenyl toward Gly321 and Met336.

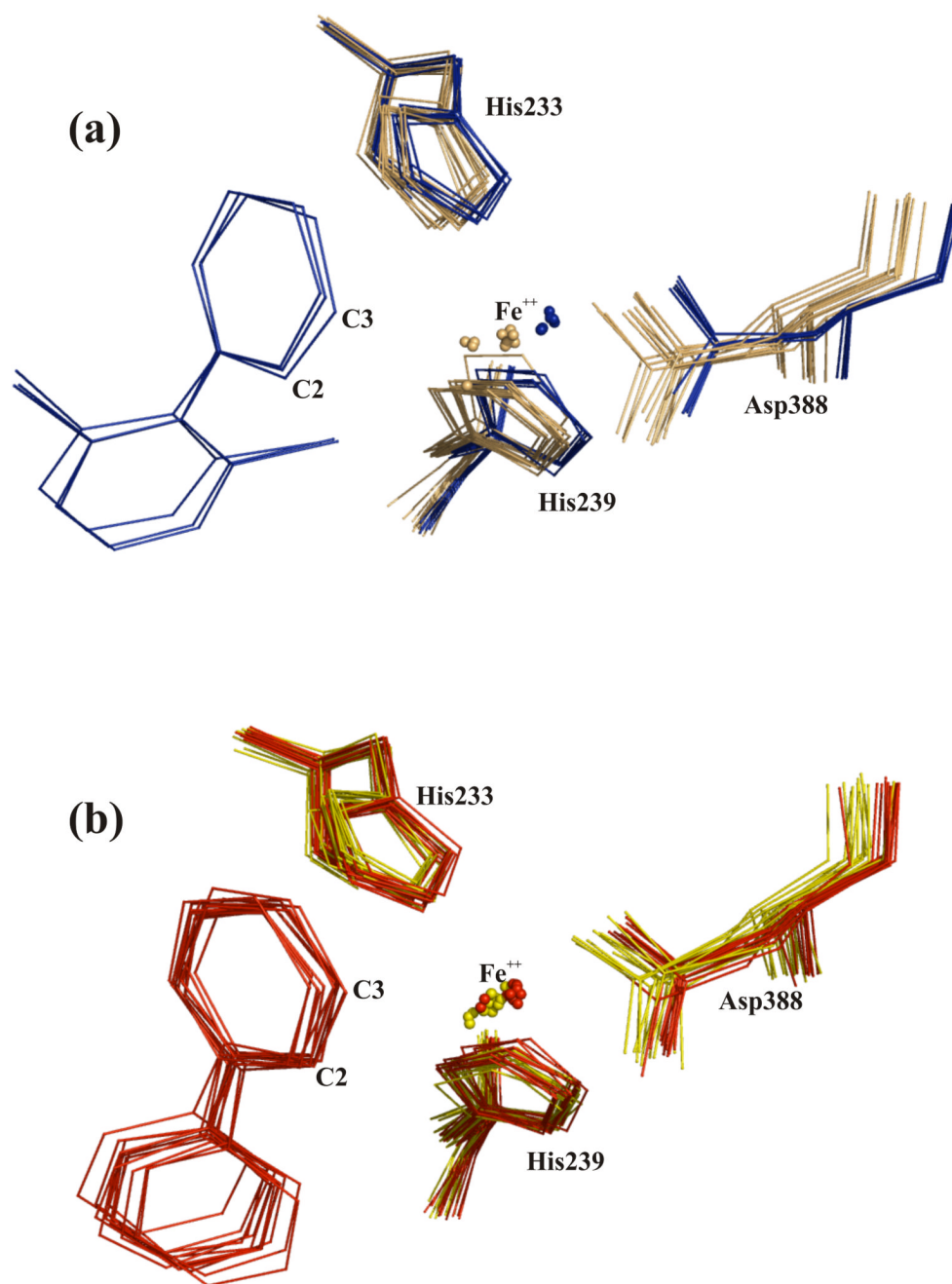


Figure 6. (a) Superposition of active site atoms from twelve BphAE_{p4} (tan) with six 2,6-dichlorobiphenyl-bound BphAE_{p4} (blue) αβ dimers and (b) superposition of twelve BphAE_{LB400} (yellow) with twelve biphenyl-bound BphAE_{LB400} (red) dimers showing the displacement of Asp388 after substrate binding.

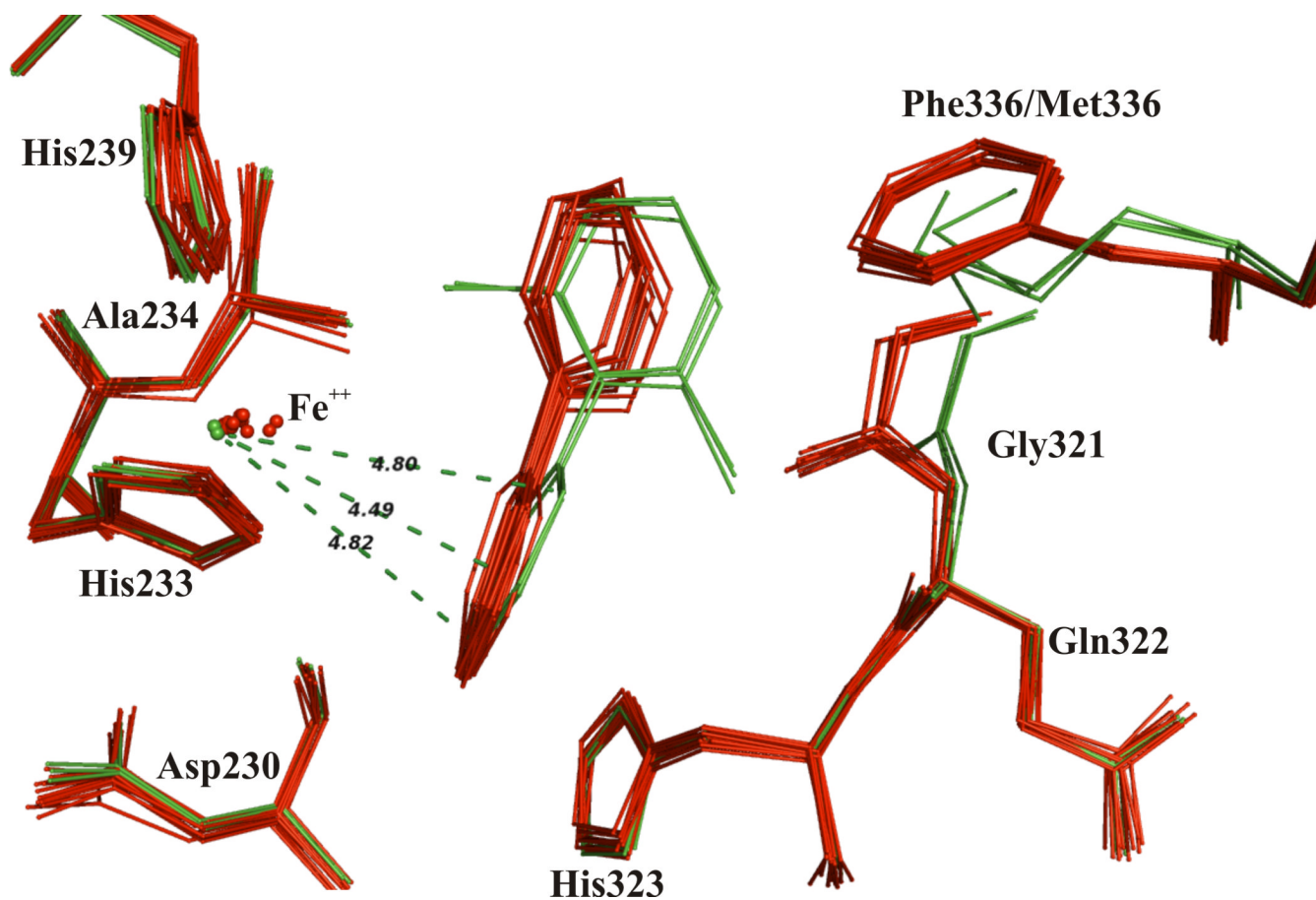


Figure 7. Superposition of twelve dimers of biphenyl-bound BphAE_{LB400} (red) with dimers AB, CD and EF of the 2,6-dichlorobiphenyl-bound BphAE_{p4} (green) showing the distances between C-2, C-3 and C-4 of 2,6-dichlorobiphenyl and the catalytic iron of dimer AB.

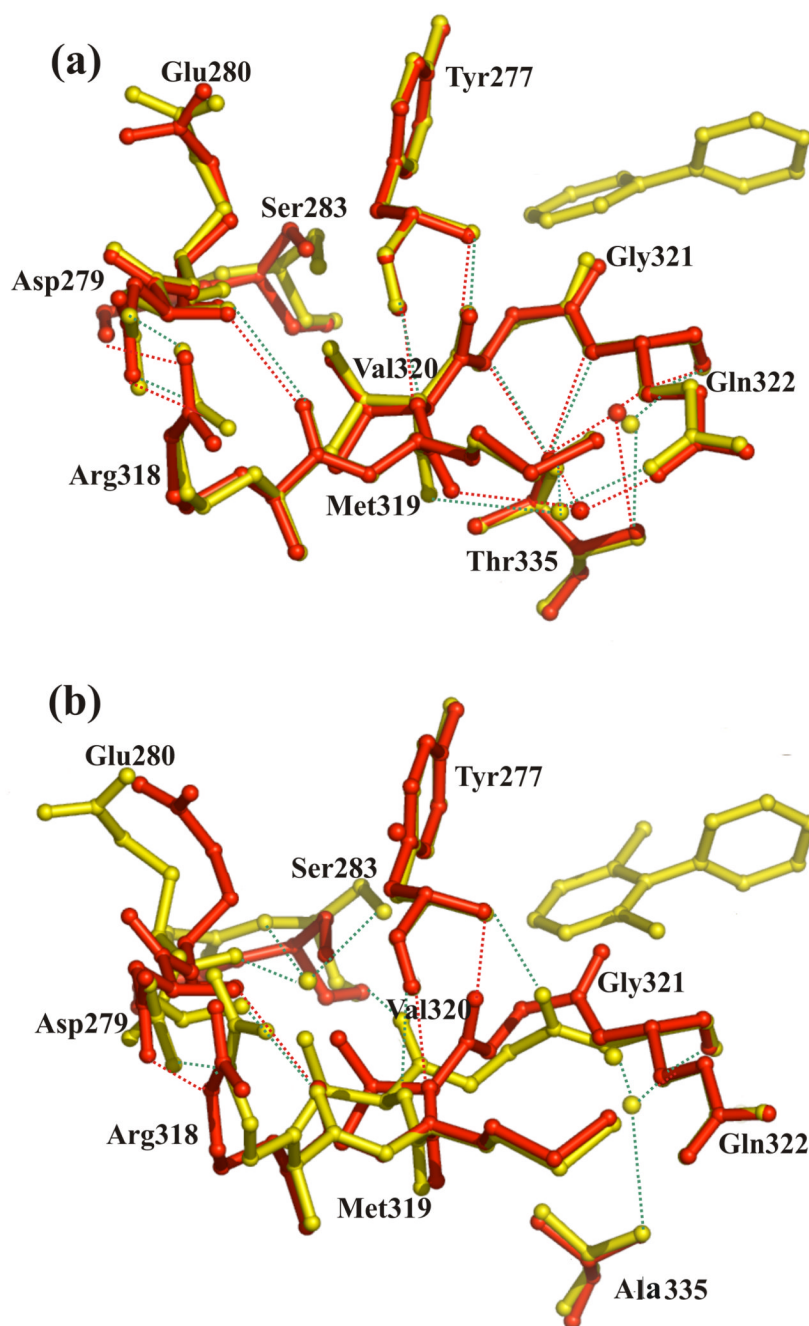


Figure 8.

(a) Superposition of segments of dimer AB of BphAE_{LB400} and of its biphenyl-bound form and (b) superposition of the corresponding segments of dimer KL of BphAE_{p4} and of dimer AB of its 2,6-dichlorobiphenyl-bound form. Both bound forms of BphAE_{LB400} and BphAE_{p4} are in yellow, native forms are in red. Dashed lines represent H-bonds of substrate complex forms (green) and of native forms (red), spheres represent water molecules.

Table 1Crystallographic data and refinement results for BphAE_{LB400} and BphAE_{p4} structures

	BphAE _{LB400}	BphAE _{LB400} : Biphenyl	BphAE _{p4}	BphAE _{p4} : 2,6-dichlorobiphenyl
Crystallographic data				
Space group	<i>P1</i>	<i>P1</i>	<i>P1</i>	<i>P2</i> ₁
Wavelength	1.0	1.0	1.0	1.0
Resolution	2.5	2.4	2.2	2.2
Cell dimensions				
<i>a</i> (Å)	132.56	132.82	133.47	86.73
<i>b</i> (Å)	132.35	132.65	133.59	276.76
<i>c</i> (Å)	132.98	130.42	133.23	93.32
α (°)	102.60	102.65	102.51	90.00
β (°)	102.69	101.11	104.99	117.37
γ (°)	104.61	105.31	102.75	90.00
Unique reflections	255418	329852	377867	177300
Completeness (%) (Last shell)	89.0 (30.0)	93.0 (74.0)	90.0 (64.3)	86.0 (51.4)
$R_{\text{sym}}(\%)^a$ (Last Shell)	10.0 (41.2)	6.5 (27.9)	6.1 (34.6)	8.0 (35.4)
I/σ (Last shell)	6.8 (1.4)	13.8 (2.2)	8.9 (2.0)	18.6 (1.5)
Multiplicity (Last shell)	2.8 (1.2)	2.7 (1.2)	2.4 (1.2)	2.6 (1.2)
Refinement				
No. of reflections (working/test)	254621/ 122731	291398/14569	358861/17943	144572/7228
No. of residues	7356	7356	7356	3678
Water molecules	2022	2014	2540	2031
Resolution range (Å)	2.5	2.4	2.2	2.2
R_{cryst} (%)	20.0	22.0	21.4	21.2
R_{free} (%)	26.8	25.6	26.6	25.3
Average <i>B</i> -factors (Å ²)	AB 47.3 CD 47.7 EF 47.4 GH 47.4 IJ 46.9 KL 47.3 MN 43.1 OP 43.2 QR 44.0 ST 52.7 UV 51.1 WX 54.1	AB 43.8 CD 43.8 EF 43.8 GH 43.8 IJ 43.8 KL 43.8 MN 43.9 OP 43.9 QR 43.9 ST 43.8 UV 43.7 WX 43.7	AB 20.4 CD 20.7 EF 20.6 GH 19.9 IJ 19.7 KL 20.6 MN 20.7 OP 16.6 QR 20.5 ST 19.9 UV 19.0 WX 22.7	AB 45.9 CD 46.5 EF 46.2 GH 46.4 IJ 47.1 KL 48.3
Water atoms	42.1	37.5	20.6	37.0

	BphAE_{LB400}	BphAE_{LB400}: Biphenyl	BphAE_{pd}	BphAE_{pd}: 2,6-dichlorobiphenyl
All atoms	47.6	43.7	20.0	46.6
rmsd on bond lengths (Å)	0.014	0.006	0.009	0.006
rmsd on bond angles (°)	1.56	0.90	1.12	0.87
Ramachandran plot (%)				
Preferred	91.7	94.7	94.9	94.8
Allowed	7.0	4.7	4.7	4.7
Outliers	1.3	0.6	0.4	0.5

a

$$R_{sym} = \frac{\sum_{hkl} \sum_{i=1}^n |I_{hkl,i} - \bar{I}_{hkl}|}{\sum_{hkl} \sum_{i=1}^n I_{hkl,i}}$$